

Confronting measured near and sub-barrier fusion cross-sections for $^{20}\text{O}+^{12}\text{C}$ with a microscopic method

R. T. deSouza,¹ S. Hudan,¹ V.E. Oberacker,² and A.S. Umar²

¹*Department of Chemistry and Center for Exploration of Energy and Matter,
Indiana University, Bloomington, Indiana 47405, USA*

²*Department of Physics and Astronomy, Vanderbilt University, Nashville, Tennessee 37235, USA*
(Dated: August 24, 2021)

Recently measured fusion cross-sections for the neutron-rich system $^{20}\text{O}+^{12}\text{C}$ are compared to dynamic, microscopic calculations using time-dependent density functional theory. The calculations are carried out on a three-dimensional lattice and performed both with and without a constraint on the density. The method has no adjustable parameters, and its only input is the Skyrme effective NN interaction. While the microscopic DC-TDHF calculations lie closer to the experimental data than standard fusion systematics they underpredict the experimental data significantly.

PACS numbers: 26.60.Gj, 25.60.Pj, 25.70.Jj, 21.60.-n, 21.60.Jz

The outer crust of an accreting neutron star provides a unique environment in which nuclear reactions can occur. It has been proposed that the fusion of two neutron-rich light nuclei in the outer crust could provide a heat source to ignite thermonuclear fusion of $^{12}\text{C} + ^{12}\text{C}$ and produce a signature X-ray superburst [1]. To date, however, a limited amount is known either experimentally or theoretically about the fusion of neutron-rich nuclei. Pioneering experiments with heavy nuclei indicate that the fusion below the barrier may be enhanced [2, 3]. Such an enhancement has recently been associated with the importance of neutron transfer channels which effectively lowers the fusion barrier [4]. In the case of fusion of two neutron-rich *light* nuclei ($Z < 20$), even less is known. In principle, this is the most promising domain as neutron-rich nuclei up to the drip line can be experimentally produced.

Recent experimental measurement of near-barrier fusion in the system $^{20}\text{O} + ^{12}\text{C}$ [5] suggests that the fusion cross-section is enhanced relative to the predictions of the Bass model [6]. As the empirical Bass model is based upon the systematics of known fusion cross-sections near β -stability, it does not include the increased importance of neutron transfer channels for neutron-rich nuclei. The aim of this paper is to directly compare the experimental results with a microscopic approach, namely the time dependent Hartree-Fock (TDHF) theory.

The experiment was performed at the SPIRAL1 facility at the GANIL accelerator complex in Caen, France. An ^{20}O beam with an intensity of $1 - 2 \times 10^4$ p/s impinged on a $100 \mu\text{g}/\text{cm}^2$ thick ^{12}C target. The energy of the beam on target was varied between 1 MeV/A and 2 MeV/A in order to measure the fusion excitation function. Experimental details have been previously published [5] and are summarized here only for completeness. Nuclei produced by fusion subsequently de-excite via evaporation of neutrons and light charged particles ($Z \leq 2$) forming evaporation residues. These residues were detected in two segmented silicon detectors located downstream of the target and identified by measuring both

their energy and time-of-flight. The annular detectors spanned the angular range $3.54^\circ \leq \theta_{lab} \leq 21.8^\circ$. Due to the presence of a large atomic background in the experiment, a coincidence between an emitted charged particle and the evaporation residue was necessary to distinguish fusion reactions. Statistical model calculations with a Hauser-Feshbach model, *evapOR*, indicate that, depending on the excitation energy of the compound nucleus formed, approximately 15-25 % of fusion reactions de-excite via emission of at least one charged particle.

The time-dependent Hartree-Fock (TDHF) theory provides a useful foundation for a fully microscopic many-body theory of large amplitude collective motion. It is therefore well suited to describing deep-inelastic and fusion reactions [7, 8]. Only in recent years has it become feasible to perform TDHF calculations on a 3D Cartesian grid without any symmetry restrictions and with much more accurate numerical methods [8–13]. In addition, the quality of effective interactions has been substantially improved [14–17]. TDHF theory predicts an energy density functional which is determined by the given effective NN interaction. One may therefore view TDHF as a special case of a time-dependent density functional theory (TDDFT), a concept used in many areas of nuclear physics, condensed-matter physics, and chemistry.

Over the past several years, the Density Constrained Time-Dependent Hartree-Fock (DC-TDHF) method for calculating heavy-ion potentials [18] was utilized to calculate fusion cross-sections. We have applied this method to calculate fusion and capture cross-sections above and below the barrier to about 20 systems to date, examples of which can be found in Refs. [19–23]. Recently, we have also investigated sub-barrier fusion between nuclei that occur in the neutron star crust [4]. In all cases, we have found good agreement between the measured fusion cross-sections and the DC-TDHF results. This agreement is rather remarkable given the fact that the only input in DC-TDHF is the Skyrme effective N-N interaction, and there are no adjustable parameters.

The TDHF equations for the single-particle wave func-

tions

$$h(\{\phi_\mu\}) \phi_\lambda(r, t) = i\hbar \frac{\partial}{\partial t} \phi_\lambda(r, t) \quad (\lambda = 1, \dots, A), \quad (1)$$

can be derived from a variational principle [7]. In the present TDHF calculations we use the Skyrme SLy4 interaction [14] for the nucleons including all of the time-odd terms in the mean-field Hamiltonian [10]. The numerical calculations are carried out on a 3D Cartesian lattice. For the calculations shown in this work, the lattice spans 40 fm along the collision axis and 24–30 fm in the other two directions, depending on the impact parameter. We first generate very accurate static HF wave functions for the two nuclei on the 3D grid. In the second step, we apply a boost operator to the single-particle wave functions. The time-propagation is carried out using a Taylor series expansion (up to orders 10–12) of the unitary mean-field propagator, with a time step $\Delta t = 0.4$ fm/c.

Presented in Fig. 1 is a contour plot of the mass density during a collision which clearly shows the formation of a neck between the two fragments. This density distribution, shown here for $^{20}\text{O}+^{12}\text{C}$ at $E_{c.m.} = 9.5$ MeV, is representative of collisions for similar systems. As the collision proceeds in the TDHF calculation, transport of protons and neutrons between the two nuclei can be followed within the theory. For larger impact parameters the larger angular momentum of the system leads the two nuclei to separate and a deep-inelastic reaction occurs. For smaller impact parameters the disrupting influence of angular momentum and Coulomb repulsion is insufficient to overcome the nuclear attraction and fusion results. By examining the density distribution as the two nuclei fuse into one within the calculation, one clearly observes the occurrence of a damped dipole resonance and surface waves. Deep inelastic and fusion reactions are the dominant reaction channels in this energy domain. Distinguishing between these two types of reactions is realized by examining the density distribution as a function of time and observing whether one or two large fragments result from the collision.

In the absence of a true quantum many-body theory of barrier tunneling, all current sub-barrier fusion calculations assume the existence of an ion-ion potential $V(R)$ which depends on the internuclear distance R . Most of the theoretical fusion studies are carried out with the coupled-channels (CC) method [24–27] in which one uses empirical ion-ion potentials (typically Woods-Saxon potentials, or double-folding potentials with frozen nuclear densities). In contrast to the use of these empirical potentials we have adopted a microscopic approach to extract heavy-ion interaction potentials $V(R)$ from the TDHF time-evolution of the dinuclear system which describes the dynamics of the underlying nuclear shell structure.

In the DC-TDHF approach [18], the TDHF time-evolution proceeds uninhibitedly. At certain times t or, equivalently, at certain internuclear distances $R(t)$ the instantaneous TDHF density is used to perform a static Hartree-Fock energy minimization while constraining the

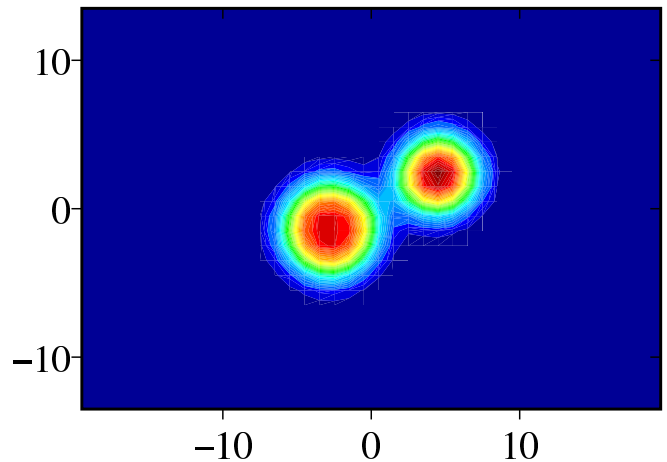


FIG. 1. (Color online) Unrestricted TDHF+BCS calculation for $^{20}\text{O}+^{12}\text{C}$ at $E_{c.m.} = 9.5$ MeV and impact parameter $b = 2.5$ fm. Shown are mass density contours shortly after a neck has formed between the two fragments.

proton and neutron densities to be equal to the instantaneous TDHF densities. This means that we allow the single-particle wave functions to rearrange themselves in such a way that the total energy is minimized, subject to the TDHF density constraint. In a typical DC-TDHF run, we utilize a few thousand time steps, and the density constraint is applied every 10–20 time steps. We refer to the minimized energy as the “density constrained energy” $E_{DC}(R)$. The ion-ion interaction potential $V(R)$ is obtained by subtracting the constant binding energies E_{A_1} and E_{A_2} of the two individual nuclei

$$V(R) = E_{DC}(R) - E_{A_1} - E_{A_2}. \quad (2)$$

In direct TDHF calculations the fusion cross-section is calculated by determining the maximum impact parameter for which fusion occurs and applying the sharp cut-off approximation. For example, in the case of the reaction $^{20}\text{O}+^{12}\text{C}$ at $E_{c.m.} = 9.5$ MeV we find that impact parameters $b \leq b_{max} = 4.075$ fm result in fusion, while impact parameters $b > b_{max}$ lead to deep-inelastic reactions. Using the sharp cut-off model, the fusion cross-section is given by $\sigma_{fus} = \pi b_{max}^2 = 52.2 \text{ fm}^2 = 522 \text{ mb}$. In contrast, in DC-TDHF method fusion cross-sections are obtained by integrating the Schrödinger equation for the potential $V(R)$ with a coordinate-dependent mass [21].

We begin the comparison of the microscopic calculations with experimental data by examining the well studied system $^{16}\text{O}+^{12}\text{C}$. Shown in Fig. 2 are four sets of experimental data for the total fusion cross-section along with the corresponding microscopic DC-TDHF calculations. The experimental techniques used to determine the fusion cross-section range from gamma spectroscopy of the charged particle channels (Christensen and Cujec) to direct measurement of the evaporation residues (Eyal and this work). It should be stressed that the data represented by the red filled circles (this work) utilized the same experimental technique and setup as for the

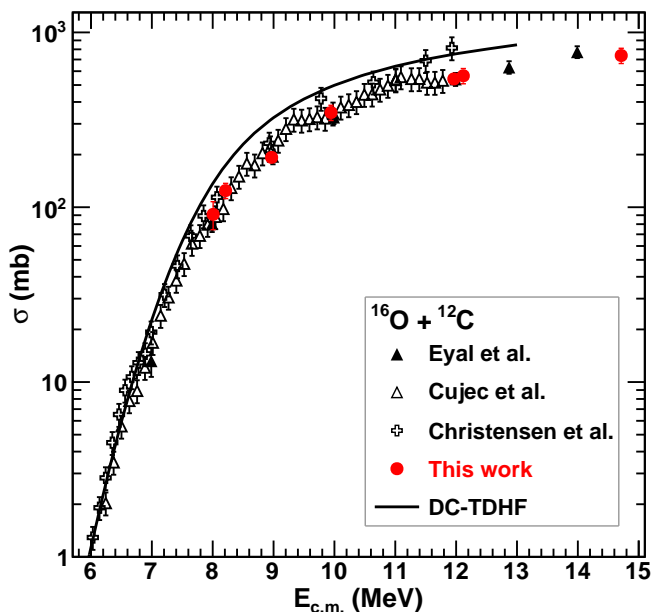


FIG. 2. (Color online) Comparison of the experimentally measured fusion excitation function with the predictions of the DC-TDHF method for $^{16}\text{O}+^{12}\text{C}$. Data from [28–30] shown.

$^{20}\text{O}+^{12}\text{C}$ results subsequently presented. For energies $E_{c.m.} < 9.5$ MeV all the experimental data are in agreement. At higher energies however, the cross-sections measured by Christensen *et al.* slightly exceed that of the three other datasets. We have no explanation at present for the larger cross-sections measured by Christensen *et al.* Since the cross-section measurements of Eyal, Cujec, and the present work are all in good agreement we take these cross-sections to accurately represent the true fusion cross-section. It is interesting to note that the DC-TDHF calculations also slightly exceed the measured cross-sections for $E_{c.m.} > 7$ MeV. At the largest energies measured this excess is of the order of 20%. Indeed, the agreement of DC-TDHF results with the data of Christensen *et al.* at the highest energies was somewhat surprising since TDHF dynamics for light heavy-ions at these energies do not properly account for various breakup channels present for these systems, and results in a fusion-like composite system with long-time collective oscillations. In coupled-channel calculations this discrepancy is cured by introducing a small imaginary potential in the vicinity of the potential minimum [27]. Having established the degree of confidence through the comparison of the fusion cross-sections in $^{16}\text{O}+^{12}\text{C}$, we then calculated fusion in $^{20}\text{O}+^{12}\text{C}$.

While for isolated ^{16}O and ^{12}C nuclei the Hartree-Fock (HF) ground state is found to be spherical in agreement with both theory and experiment, for ^{20}O the HF calculations predict a prolate quadrupole deformation of $\beta_2 = 0.25$. This deformation is in disagreement with self-consistent mean field calculations with pairing (Skyrme-HFB) [31] which predict a spherical nucleus. Moreover,

the measured energy level spectrum [32] also shows this nucleus to be spherical. In addition, a measurement of the magnetic moment of ^{20}O [33] also indicates its spherical nature. We attribute this prolate deformation predicted by the HF calculations to the lack of pairing in the method. One unfortunate consequence of the DC-TDHF approach in calculating the fusion cross-section lies in the treatment of pairing during the collision process. In unrestricted TDHF calculations, the BCS occupation numbers can be kept frozen during the collision to have correct initial states. This approximation cannot be utilized in the DC-TDHF method because the static HF solution coupled with a constraint on the instantaneous TDHF density for the combined system requires the reevaluation of the occupation numbers for the lowest energy solution. Consequently, calculations with the DC-TDHF method do not include pairing. On qualitative grounds, it can be argued that this omission should result in a slightly larger prediction of the fusion cross-section. The reason is that pairing results in a spherical ^{20}O nucleus, and the fusion barrier for a spherical nucleus is higher than the lowest barrier for a deformed nucleus. In order to calculate the fusion cross-section for this system within DC-TDHF method we therefore take an average of all initial orientation angles β of the deformed ^{20}O nucleus, where β is defined as the angle between the internuclear distance vector and the symmetry axis of the deformed nucleus.

As the collision occurs, using TDHF dynamics, it is possible to compute the corresponding coordinate dependent mass parameter $M(R)$ [21]. At large distance R , the mass $M(R)$ is equal to the reduced mass μ of the system. At smaller distances, when the nuclei overlap, the mass parameter generally increases. In order to calculate the fusion cross-section more easily, one can replace the coordinate-dependent mass $M(R)$ and the original potential $V(R)$ with the constant mass μ and the “transformed potential” $U(\bar{R})$, using a scale transformation [21]. In Fig. 3 we display the transformed potentials $U(\bar{R})$ for initial orientation angles $\beta = 0^\circ, 10^\circ, \dots, 90^\circ$ of ^{20}O . For sufficiently large separation between the two nuclei, $R \geq 9$, fm all the transformed heavy-ion potentials are the same regardless of the orientation of the two nuclei. With decreasing distance as the two nuclei come into contact, the heavy-ion potentials differ. For a nucleus with prolate deformation, the orientation angle $\beta = 0^\circ$ leads to the lowest potential barrier. This reduction in the potential occurs because the distance between the nuclear surfaces is minimized for this orientation which is important because of the short-range nature of the strong interaction. The Coulomb interaction is accurately calculated by solving the 3D Poisson equation numerically during the collision. We observe that with increasing orientation angle, the barrier height increases and the barrier position is shifted to smaller distances.

Displayed in the inset of Fig. 3 is the fusion excitation function associated with the orientations of $\beta=0^\circ$ and 90° as well as the angle averaged result. As one might quali-

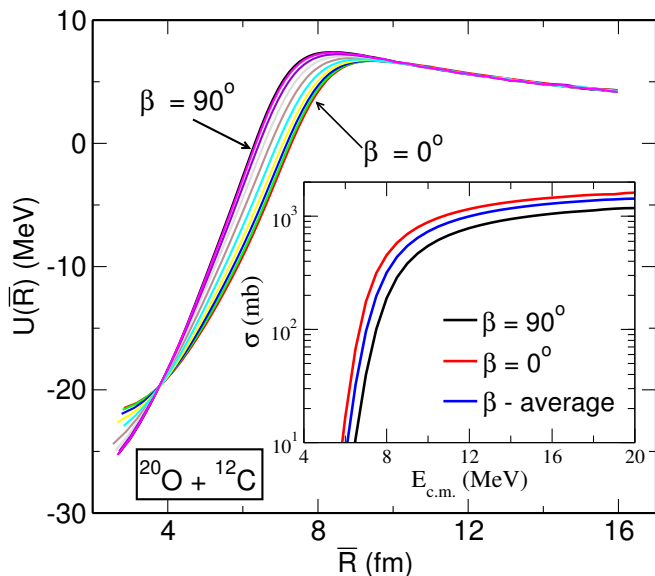


FIG. 3. (Color online) Transformed heavy-ion potentials $U(\bar{R})$, corresponding to the constant reduced mass μ . The potentials have been calculated for a series of initial orientation angles β of the deformed ^{20}O nucleus (no pairing). Shown in the inset is the total predicted cross-section as a function of $E_{c.m.}$ for $\beta=0^\circ$, $\beta=90^\circ$, as well as the cross-section averaged over β .

tatively expect, based upon the heavy-ion potentials, for a given $E_{c.m.}$, the orientation $\beta = 0^\circ$ with the lowest potential barrier corresponds to the largest cross-section.

In Fig. 4 we compare the microscopic calculations using the DC-TDHF method to the experimental data. The experimental data at $E_{c.m.} = 7.35, 9.29,$ and 15.24 MeV are shown as the filled circles. Due to the atomic background previously mentioned only the fraction of the fusion cross-section associated with subsequent charged particle emission was experimentally measured. In order to compare the microscopic calculations with the experimental data, we therefore calculated the fraction of compound nuclei produced at each incident energy that de-excite via emission of at least one charged particle. To calculate the de-excitation of the fused nuclei we utilized a Hauser-Feshbach statistical model, *evapor*. The theoretically predicted fusion cross-section associated with subsequent charged particle channels is depicted by the dashed line. This predicted cross-section clearly underpredicts the experimentally measured cross-section. At the highest energy, $E_{c.m.} = 15.24$ MeV, the predicted cross-section is 60 % of the experimentally measured one while at the lowest energy the predicted cross-section is substantially lower, only 30 % of the experimental value. For reference, we also present, as a dot-dash line, the fusion cross-section predicted by the Bass systematics that is associated with charged particle emission. This cross-section is less than that of the DC-TDHF method most likely reflecting the influence of neutron transfer channels in aiding the fusion process. It should be appreci-

ated that not only does the DC-TDHF method predict a larger cross-section at all energies as compared to the Bass systematics, but this increase grows with decreasing $E_{c.m.}$. This result suggests that the neutron transfer becomes more important in the sub-barrier domain. The result that the DC-TDHF method underpredicts the experimental data by a significant amount is noteworthy. Moreover, it should be noted that the lack of pairing in the DC-TDHF method and the resulting deformation of the ^{20}O , as previously discussed, acts to increase the predicted cross-section implying that the discrepancy between theoretical prediction and experimental data is at least as large as that evident in Fig. 4.

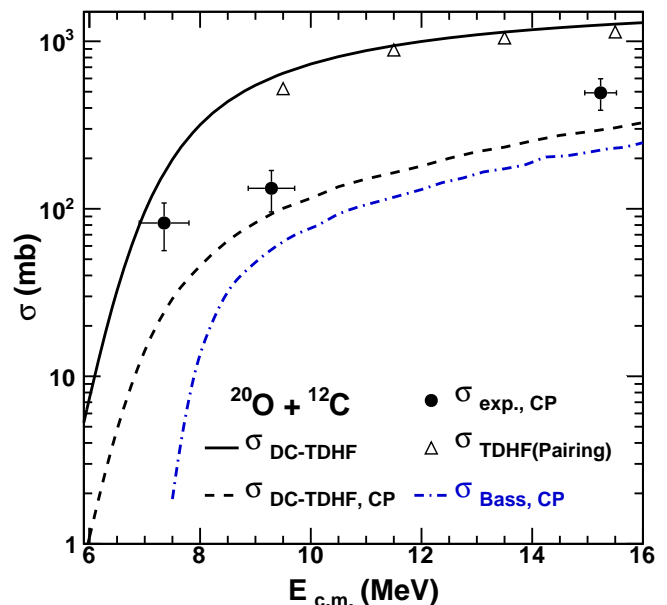


FIG. 4. (Color online) Comparison of the angle-averaged DC-TDHF fusion cross-sections with experimental data for $^{20}\text{O} + ^{12}\text{C}$.

In order to assess the impact of pairing on the measured cross-sections more quantitatively we have performed unrestricted TDHF calculations (no barrier tunneling) at energies above the barrier. These calculations were initialized with BCS/Lipkin-Nogami pairing for ^{20}O which resulted in a spherical nucleus, consistent with the experimental data. During the collision of the ^{20}O with the ^{12}C the BCS occupation numbers are kept frozen. The results of these calculations are presented as the open triangles in Fig. 4. A slight reduction in the total cross-section is evident. This reduction is of the order of 5-20 % with the largest reduction for the lowest energy point calculated. From these calculations one can infer that the inclusion of pairing in the DC-TDHF calculations should result in a slight reduction of the predicted cross-section, thus increasing the discrepancy with the experimental data as anticipated.

It is tantalizing to speculate about possible reasons for the discrepancy between the theoretical predictions and

the experimental data. In general terms, the discrepancy between the experimental data for the charged particle channels in Fig. 4 (solid points) and the corresponding DC-TDHF calculations can be thought of as originating either from an underprediction of the total fusion cross-section or from an underestimation of the relative importance of the charged particle decay in the de-excitation of the compound nucleus. Either or both of these sources could explain the underprediction of the cross-section. It is therefore important to not only measure the total fusion cross-section but also the cross-section for individual decay channels. Furthermore, since the underprediction exists for energies well above the barrier, $E \approx 9.5$ MeV, it is not simply a question of enhanced tunneling. Moreover, beyond the overall underprediction of the microscopic method, one observes that the experimental data

manifests a slower fall-off for the measured cross-section with decreasing incident energy as compared to the DC-TDHF calculations. This experimentally determined energy dependence is highly provocative and it remains to be seen whether the total fusion cross-section also exhibits this slower fall-off. As this fall-off is intimately related to the neutron transfer channels, near and sub-barrier fusion of neutron-rich nuclei provides direct access to the extent of the neutron density distribution.

ACKNOWLEDGMENTS

This work has been supported by the U.S. Department of Energy under Grant No. DE-FG02-96ER40975 (Vanderbilt University) and DE-FG02-88ER-40404 (IU).

-
- [1] C. J. Horowitz, H. Dussan, and D. K. Berry, *Phys. Rev. C* **77**, 045807 (2008).
 - [2] W. Loveland *et al.*, *Phys. Rev. C* **74**, 064609 (2006).
 - [3] J. F. Liang *et al.*, *Phys. Rev. C* **85**, 031601(R) (2012).
 - [4] A. S. Umar, V. E. Oberacker, and C. J. Horowitz, *Phys. Rev. C* **85**, 055801 (2012).
 - [5] M. J. Rudolph *et al.*, *Phys. Rev. C* **85**, 024605 (2012).
 - [6] R. Bass, *Phys. Rev. Lett.* **39**, 265 (1977).
 - [7] J. W. Negele, *Rev. Mod. Phys.* **54**, 913 (1982).
 - [8] C. Simenel, *Phys. Rev. Lett.* **106**, 112502 (2011).
 - [9] A. S. Umar *et al.*, *Phys. Rev. C* **44**, 2512 (1991).
 - [10] A. S. Umar and V. E. Oberacker, *Phys. Rev. C* **73**, 054607 (2006).
 - [11] C. Simenel, *Eur. Phys. J. A* **48**, 152 (2012).
 - [12] L. Guo, J. A. Maruhn, P.-G. Reinhard, and Y. Hashimoto, *Phys. Rev. C* **77**, 041301(R) (2008).
 - [13] K. Washiyama and D. Lacroix, *Phys. Rev. C* **78**, 024610 (2008).
 - [14] E. Chabanatand *et al.*, *Nucl. Phys. A* **643**, 441(E) (1998).
 - [15] P. Klüpfel, P.-G. Reinhard, T. J. Bürvenich, and J. A. Maruhn, *Phys. Rev. C* **79**, 034310 (2009).
 - [16] M. Kortelainen *et al.*, *Phys. Rev. C* **82**, 024313 (2010).
 - [17] A. S. Umar, M. R. Strayer, and P.-G. Reinhard, *Phys. Rev. Lett.* **56**, 2793 (1986).
 - [18] A. S. Umar and V. E. Oberacker, *Phys. Rev. C* **74**, 021601(R) (2006).
 - [19] A. S. Umar and V. E. Oberacker, *Phys. Rev. C* **74**, 061601(R) (2006).
 - [20] A. S. Umar and V. E. Oberacker, *Phys. Rev. C* **76**, 014614 (2007).
 - [21] A. S. Umar and V. E. Oberacker, *Eur. Phys. J. A* **39**, 243 (2009).
 - [22] A. S. Umar, V. E. Oberacker, J. A. Maruhn, and P.-G. Reinhard, *Phys. Rev. C* **81**, 064607 (2010).
 - [23] R. Keser, A. S. Umar, and V. E. Oberacker, *Phys. Rev. C* **85**, 044606 (2012).
 - [24] K. Hagino and Y. Watanabe, *Phys. Rev. C* **76**, 021601(R) (2007).
 - [25] M. Dasgupta *et al.*, *Phys. Rev. Lett.* **99**, 192701 (2007).
 - [26] T. Ichikawa, K. Hagino, and A. Iwamoto, *Phys. Rev. Lett.* **103**, 202701 (2009).
 - [27] H. Esbensen, C. L. Jiang, and A. M. Stefanini, *Phys. Rev. C* **82**, 054621 (2010).
 - [28] B. Cujec and C. A. Barnes, *Nucl. Phys. A* **266**, 461 (1976).
 - [29] Y. Eyal *et al.*, *Phys. Rev. C* **13**, 1527 (1976).
 - [30] P. R. Christensen, Z. E. Switkowski, and R. A. Dayras, *Nucl. Phys. A* **280**, 189 (1977).
 - [31] J. Dobaczewski, M. V. Stoitsov, and W. Nazarewicz, in *AIP Conference Proceedings Volume*, Vol. 726, edited by R. Bijker, R. Casten, and N. Y. A. Frank (American Institute of Physics (2004) p. 51, nucl-th/0404077).
 - [32] D. R. Tilley *et al.*, *Nucl. Phys. A* **636**, 249 (1998).
 - [33] J. Gerber, M. B. Goldberg, and K.-H. Speidel, *Phys. Lett. B* **60**, 338 (1976).